https://doi.org/10.5194/egusphere-2026-4127
Preprint. Discussion started: 31 August 2026

An Explainable Machine Learning Perspective on Anthropogenic Emission and Meteorology drivers of long-term $PM_{2.5}$ Trends over Northeast China

Zhongfeng Pan[1], Hao Yin[2,*], Haolin Wang[3], Zhenda Sun[4], Chongyang Li[4], Yu Yang[5], Youwen Sun[1,4,6,*]

[1] School of Optoelectronic Science and Engineering, Anhui University, Hefei 230601, China

[2] School of Energy and Environment, City University of Hong Kong, Hong Kong SAR, China

[3] School of GeoSciences, University of Edinburgh, Edinburgh, United Kingdom

[4] Key Laboratory of Environmental Optics and Technology, Anhui Institute of Optics and Fine Mechanics, HFIPS, Chinese Academy of Sciences, Hefei 230031, China

[5] Department of Data Science, City University of Hong Kong, Hong Kong SAR, China

[6] School of Environmental Science and Optoelectronic Technology, University of Science and Technology of China, Hefei 230026, China

Corresponding author: Youwen Sun (ywsun@ahu.edu.cn); Hao Yin (haoyin@cityu.edu.hk)

Abstract

Northeast China is a cold industrial and agricultural region where $PM_{2.5}$ pollution is influenced by emission changes, winter heating, agricultural burning, and meteorological variability, but long-term city-level evidence of these drivers remains limited. Here we combined hourly $PM_{2.5}$ observations from 36 cities during 2015–2025 with ERA5 meteorology, LightGBM models interpreted using Shapley Additive Explanations, and weather normalization. Observed $PM_{2.5}$ was separated into a weather-normalized component (PM_{emi}), representing non-meteorological variability in the pollution baseline, and a meteorological modulation term (PM_{met}). Regional annual mean $PM_{2.5}$ decreased by 39.7%, from 48.4 μg m^{-3} in 2015 to 29.2 μg m^{-3} in 2025. The PM_{emi} trend accounted for 95.5% of the observed linear decrease and showed consistent decreases with independent CEDS emission indices, supporting an important role of anthropogenic emission reductions. However, regional annual mean $PM_{2.5}$ changed little after 2022 and remained above 25 μg m^{-3}. Regional exceedance days decreased from 52 to 12 d yr^{-1}, but PM_{met} was positive on all 229 exceedance days, indicating meteorological amplification during high-pollution episodes. Model interpretation further linked exceedance-day $PM_{2.5}$ enhancement to thermal, pressure, moisture, wind, and boundary-layer conditions. VIIRS fire detections and CO observations indicated that agricultural biomass burning and other combustion sources were associated with short-term $PM_{2.5}$ variability during spring and autumn

https://doi.org/10.5194/egusphere-2026-4127
Preprint. Discussion started: 31 August 2026

burning seasons. These results show how emission reductions, residual combustion sources, and unfavorable meteorology jointly control $PM_{2.5}$ variability in cold industrial and agricultural regions.

1. Introduction

Fine particulate matter ($PM_{2.5}$) remains a major atmospheric pollutant due to its complex composition, prolonged atmospheric lifetime, and adverse effects on visibility, climate, and human health (Zhang et al., 2022; WHO, 2021). In Northeast China, fine particles have been closely associated to visibility degradation and regional air quality deterioration, particularly during haze episodes (Zhao et al., 2013; Li et al., 2017). $PM_{2.5}$ variability across China is jointly driven by primary emissions, secondary aerosol formation, and meteorological conditions, which complicates the attribution of observed concentration changes solely to anthropogenic emissions (Wang et al., 2014; Xiao et al., 2021; Zhang et al., 2015)

Northeast China, including Liaoning, Jilin, and Heilongjiang provinces, is a critical target region for investigating $PM_{2.5}$ variability due to that it uniquely combines a traditional industrial base, a major grain-production region, and one of the coldest populated regions in China (Chen et al., 2018). The region undergoes an extended heating season lasting approximately 4–6 months, during which residential heating, small coal-fired boilers, and industrial energy consumption substantially elevate combustion-related emissions (Bai et al., 2021). Wintertime haze studies have demonstrated that $PM_{2.5}$ concentrations in Northeast China can increase markedly during this period, with coal combustion, primary organic aerosols, and the formation of secondary sulfate, nitrate, and ammonium acting as major contributors to haze development (Zhang et al., 2017). These effects are exacerbated by unfavorable meteorological conditions, including stable synoptic conditions, low boundary-layer height, high relative humidity, low wind speed, and temperature inversion, which further promote $PM_{2.5}$ accumulation, secondary transformation, and visibility degradation during winter pollution episodes (Liu et al., 2021; Ma et al., 2018). In addition to industrial and heating-related emissions, agricultural burning is another defining feature of this region. As a major grain-producing area, post-harvest straw burning and open biomass burning can trigger sharp increases in $PM_{2.5}$ during autumn and spring pollution episodes over Northeast China (Yang et al., 2020). For example, Huang et al. (2024) showed that biomass burning in Northeast China is concentrated mainly in March–April and October–November, is dominated by cropland fires, and is positively associated with ground-observed $PM_{2.5}$, PM_{10}, and CO. Despite these recognized regional characteristics, systematic evidence for Northeast China remains limited compared with more extensively studied regions such as the North China Plain, eastern China, and the Yangtze River Delta (Zhai et al., 2019; Zhen et al., 2023). Existing studies have provided important insights into winter haze formation, biomass burning episodes, and meteorological influences in Northeast China,

https://doi.org/10.5194/egusphere-2026-4127
Preprint. Discussion started: 31 August 2026

but most of them have focused on specific seasons, individual pollution episodes, or selected cities. For a region characterized by heavy winter heating demand, frequent agricultural biomass burning, and strong seasonal meteorological contrasts, there is still a lack of long term, city level evidence that combines weather normalization with multiple independent indicators to evaluate the relative roles of emission changes, meteorological modulation, and episodic burning.

Since observed $PM_{2.5}$ variations are driven by changes in both anthropogenic emissions and meteorological conditions, concentration trends cannot be straightforwardly attributed to non-meteorological factors. Previous studies have shown that meteorological adjustment can reduce the confounding influence of weather variability and yield a more comparable signal for air quality trend analysis (Grange et al., 2018; Sun et al., 2021; Vu et al., 2019; Zheng et al., 2023). Consequently, a rigorous method capable of decoupling the respective contributions of meteorology and emissions is highly desirable (Yin et al., 2022a). Such an approach is essential not only for quantifying the genuine impacts of emission reduction policies and elucidating the underlying drivers of regional pollution, but also for providing critical benchmarks for environmental assessments and future atmospheric policy development (Sun et al., 2021; Yin et al., 2021a, b).

Machine learning has been increasingly applied to $PM_{2.5}$ modeling because it can integrate observations, meteorological variables, and other predictors while capturing nonlinear relationships in large air quality datasets (Ma et al., 2020; Xiao et al., 2018; Zhong et al., 2021). Among tree ensemble models, LightGBM is well suited for large scale $PM_{2.5}$ modeling because of its histogram based decision tree learning and leaf wise tree growth strategy, which improve training efficiency while maintaining predictive performance (Yin et al., 2022b). Its successful application in national scale hourly $PM_{2.5}$ reconstruction also supports its capability for handling high frequency and large sample air quality datasets (Ke et al., 2017). However, high predictive accuracy alone is insufficient for atmospheric interpretation. This limitation is particularly relevant for Northeast China, where $PM_{2.5}$ variability is affected by strong seasonal meteorological contrasts, winter heating emissions, boundary layer changes, humidity, stagnant conditions, and episodic agricultural burning. These interacting factors make it difficult to distinguish emission-related changes from meteorological modulation using concentration trends alone. Shapley Additive Explanations (SHAP) provide an additive attribution framework for explaining individual model predictions (Lundberg and Lee, 2017), and have been widely used in interpretable air pollution studies to identify key atmospheric drivers (Hou et al., 2022; Houdou et al., 2023; Yin et al., 2026). Therefore, combining LightGBM, weather normalization, and SHAP interpretation provides a practical framework for reproducing hourly $PM_{2.5}$ variability and for separating weather-normalized and meteorology-related components in Northeast China.

https://doi.org/10.5194/egusphere-2026-4127
Preprint. Discussion started: 31 August 2026

In this study, we developed an explainable machine learning and meteorological normalization framework to investigate $PM_{2.5}$ variability across 36 prefecture level cities in Northeast China from 2015 to 2025. Hourly surface $PM_{2.5}$ observations and ERA5 meteorological variables were used to train separate LightGBM models for each city, and SHAP analysis was applied to interpret the meteorological and temporal sensitivities learned by the models. A meteorological normalization procedure was then employed to decompose the observed $PM_{2.5}$ into a meteorologically normalized component (PM_{emi}), and a meteorological modulation term, (PM_{met}). PM_{emi} was interpreted as the non-meteorological component associated with changes in the pollution baseline, rather than as a direct emission inventory. Independent CEDS emission indices, VIIRS active fire detections, and CO observations were further used to evaluate whether PM_{emi} was consistent with anthropogenic emissions, biomass burning activity, and combustion related indicators.

Based on this framework, this study aimed to: (1) characterize the long term changes and spatial heterogeneity of surface $PM_{2.5}$ in Northeast China; (2) examine whether the observed $PM_{2.5}$ decline was mainly retained in PM_{emi} or driven by meteorological modulation; (3) compare PM_{emi} with independent CEDS emission indices to evaluate the role of anthropogenic emission reductions; (4) assess the episodic influence of agricultural biomass burning during the main burning seasons; and (5) identify the role of unfavorable meteorological conditions in regional $PM_{2.5}$ exceedance events. This study provides a regional assessment of $PM_{2.5}$ drivers in Northeast China and offers evidence for air quality management in old industrial, cold climate, and agricultural regions.

2. Data Source

2.1 Observational data from national monitoring sites

Ground-level air pollutant observations were obtained from the China National Environmental Monitoring Center (CNEMC; https://www.cnemc.cn/, last access: 31 December 2025). Hourly concentrations of $PM_{2.5}$ and CO from 2015 to 2025 were collected for 36 prefecture-level cities in Northeast China, covering Liaoning, Jilin, and Heilongjiang provinces. The spatial distribution of the study cities and national air-quality monitoring stations is shown in FigureS1 The geographic information of the 36 cities detailed city-level station information are provided in Table S1 and S2, respectively. To avoid ambiguity in city names, Chaoyang City in Liaoning Province is denoted as ChaoyangLN, and Yichun City in Heilongjiang Province is denoted as YichunHLJ throughout this study.

The monitoring network comprises 167 national air-quality monitoring stations. For cities with multiple monitoring station, hourly observations from all available stations within the same city were averaged to obtain city-level pollutant concentrations. $PM_{2.5}$ was used as the target variable for model training, meteorological normalization, and long-term trend analysis. CO

https://doi.org/10.5194/egusphere-2026-4127
Preprint. Discussion started: 31 August 2026

was excluded from the model training and served solely as an independent combustion-related indicator to evaluate the consistency of the weather-normalized $PM_{2.5}$ component (PM_{emi}).

The national monitoring stations follow unified technical specifications for automatic ambient air-quality monitoring in China, including standardized instrument operation, calibration, and quality-control procedures. $PM_{2.5}$ is measured using automatic particulate monitoring methods, while CO is measured using non-dispersive infrared absorption. These standardized procedures ensure the comparability and long-term consistency of air pollutant observations across the regional monitoring network.

2.2 ERA5 meteorological data

Hourly meteorological data were obtained from the ERA5 reanalysis dataset produced by the European Centre for Medium-Range Weather Forecasts (ECMWF) and accessed through the Copernicus Climate Data Store (https://cds.climate.copernicus.eu, last access: 31 December 2025). ERA5 provides globally consistent atmospheric and land-surface meteorological fields at an hourly temporal resolution, and the data used in this study were retrieved on a 0.25° × 0.25° regular latitude–longitude grid (Hersbach et al., 2020).

In this study, the ERA5 meteorological predictors included boundary layer height (BLH), 2 m dewpoint temperature (T_d), surface pressure (p_s), surface short-wave radiation downwards (SSRD), 2 m air temperature (T), total cloud cover (TCC), total precipitation (TP), and 10 m zonal and meridional wind components (u_{10} and v_{10}). The corresponding original ERA5 variable names are provided in Table S3. Relative humidity (RH) was calculated from T and T_d and was also included to represent near-surface moisture conditions.

The physical meaning, units, and variable types of the ERA5 predictors are summarized in Table S3. Among these variables, SSRD and TP are accumulated fields and were treated as hourly accumulated short-wave radiation and precipitation, respectively, whereas the other ERA5 variables are instantaneous fields. Together, these variables characterize thermal conditions, humidity, boundary-layer mixing, precipitation removal, cloud cover, radiation, surface pressure, and near-surface wind conditions relevant to $PM_{2.5}$ variability.

2.3 CEDS emission inventory

Anthropogenic emission data were obtained from the Community Emissions Data System (CEDS), a global gridded emission inventory that provides temporally resolved, sector-specific anthropogenic emissions of reactive gases and aerosols (Hoesly et al., 2018). The CEDS data used in this study have a monthly temporal resolution and a spatial resolution of 0.5° × 0.5°. In this study, CEDS emissions were not used as predictors in the LightGBM model, but were used as independent emission-related information to evaluate the consistency of the weather-normalized $PM_{2.5}$ component.

https://doi.org/10.5194/egusphere-2026-4127
Preprint. Discussion started: 31 August 2026

Considering the formation pathways of fine particulate matter, five $PM_{2.5}$-related emission species were selected from CEDS, including BC, OC, SO_2, NO, and NH_3. BC and OC represent primary carbonaceous particulate emissions and are closely related to combustion sources, while SO_2, NO, and NH_3 are important precursors of secondary inorganic aerosols. Annual emission indices were calculated over Northeast China based on these species and were compared with the annual weather-normalized $PM_{2.5}$ index. Specifically, CEDS grid-cell emission fluxes were first integrated within each city polygon using grid-cell area and fractional overlap, and the resulting city-total emissions were then summed across the 36 cities to obtain the regional emission total for Northeast China. The regional CEDS emission totals were normalized to the 2015 level to construct annual emission indices. This comparison was used to examine whether the weather-normalized component derived from the machine learning framework was consistent with independent anthropogenic emission inventory information.

2.4 VIIRS active fire data

Satellite-detected active fire data were used as an external indicator of biomass-burning activity in Northeast China. Active fire detections from the VIIRS sensor onboard the Suomi National Polar-orbiting Partnership satellite were collected for 2015–2025 (Schroeder et al., 2014). In this study, the number of active fire detections was used to represent the occurrence frequency of regional fire activity.

For each city, active fire detections within a 100 km radius of the city center were summarized to characterize the potential influence of surrounding biomass-burning activity on urban $PM_{2.5}$ variability. These fire-count data were not used as predictors in the LightGBM model, but were used to support the interpretation of the weather-normalized $PM_{2.5}$ component and to examine whether non-meteorological $PM_{2.5}$ variability was associated with regional fire activity.

2.5 Spatial aggregation and city-level alignment

The machine-learning dataset was constructed at the city-hour scale rather than at the monitoring-station or grid-cell scale. Hourly $PM_{2.5}$ and CO observations had already been aggregated to city-level time series by averaging all available national monitoring stations within each city; these observations were not interpolated or gridded to the ERA5 or CEDS grids.

For ERA5 meteorological variables, prefecture-level city polygons were overlaid with the 0.25° × 0.25° ERA5 grid. Grid cells whose center points fell within each city polygon were selected, and their hourly values were arithmetically averaged to obtain city-level meteorological predictors. Therefore, a city could be represented by one or multiple ERA5 grid cells, and the number of grid cells varied among cities depending on city area and geometry. If no ERA5 grid-cell center fell within a city polygon, the grid cell nearest to the polygon centroid was assigned to that city.

https://doi.org/10.5194/egusphere-2026-4127
Preprint. Discussion started: 31 August 2026

For CEDS emissions, monthly grid-cell emission fluxes were integrated within each city polygon using grid-cell area and fractional overlap. The resulting city-total emissions were then summed across the 36 cities to obtain regional emission totals for Northeast China. CEDS emissions were not used as predictors in the LightGBM model, but were used as independent emission-related information to evaluate the consistency of the weather-normalized $PM_{2.5}$ component. This procedure ensured that the observational and meteorological inputs used for model training and weather normalization were spatially aligned at the city-hour scale, while CEDS emissions were aligned with the regional annual $PM_{2.5}$ decomposition results for external comparison.

3. Machine Learning Framework

3.1 Feature engineering

For each city, hourly $PM_{2.5}$ observations, ERA5 meteorological variables, and temporal descriptors were organized into a city-hour modeling dataset. Temporal features were first constructed to represent long-term and periodic variations in $PM_{2.5}$. A continuous time index, represented by Unix timestamp, was used to describe the long-term temporal progression during 2015–2025. The day_of_week variable was included to capture weekly variability. To represent the annual cycle while avoiding artificial discontinuity between December and January, the month was transformed into two harmonic terms:

$$\text{month\_sin} = \sin\left(\frac{2\pi m}{12}\right) \tag{1}$$

$$\text{month\_cos} = \cos\left(\frac{2\pi m}{12}\right) \tag{2}$$

where m represents the month of the year.

Meteorological predictors were then introduced to describe atmospheric conditions relevant to $PM_{2.5}$ variability. These predictors included BLH, T_d, p_s, SSRD, T, TCC, TP, u_{10}, and v_{10}. In addition, RH was derived from T and T_d to represent near-surface moisture conditions. Because T and T_d are provided in Kelvin in ERA5, they were first converted to degrees Celsius before calculating RH. The saturation vapor pressure and actual vapor pressure were estimated using the Magnus formula as follows:

$$e_s(T) = 6.1094 \times \exp\left(\frac{17.625 \times T}{243.04 + T}\right) \tag{3}$$

$$e_a(T_d) = 6.1094 \times \exp\left(\frac{17.625 \times T_d}{243.04 + T_d}\right) \tag{4}$$

where T and T_d represent the 2 m air temperature and 2 m dewpoint temperature in degrees

https://doi.org/10.5194/egusphere-2026-4127
Preprint. Discussion started: 31 August 2026

Celsius, respectively. $e_s(T)$ denotes the saturation vapor pressure at air temperature, and $e_a(T_d)$ denotes the actual vapor pressure estimated from dewpoint temperature.

Relative humidity was then calculated as:

$$\mathrm{RH} = 100 \times \frac{e_a(T_d)}{e_s(T)} \tag{5}$$

The calculated RH values were constrained to the range of 0–100 %. The final predictor set consisted of temporal descriptors, original ERA5 meteorological variables, and derived relative humidity. CO, CEDS emissions, and VIIRS fire counts were not used as model predictors, but were retained for external comparison and interpretation.

3.2 Model training and cross-validation procedure

Before model fitting, records with invalid timestamps or missing $PM_{2.5}$ observations were removed. Missing or infinite values in the predictor variables were imputed within each training-validation split using the median value calculated from the training subset. The same training-derived median was then applied to the corresponding validation subset to avoid information leakage during preprocessing.

A LightGBM regression model was independently trained for each city using hourly $PM_{2.5}$ as the target variable and the predictors described in the Feature engineering subsection as model inputs. Hyperparameter optimization was performed separately for each city using a randomized search over predefined parameter ranges. The optimized hyperparameters controlled the number of boosting iterations, learning rate, tree complexity, minimum number of samples required in a child leaf, row and feature subsampling fractions, and L1 and L2 regularization strengths. Specifically, tree complexity was controlled by the number of leaves and maximum tree depth, and regularization was controlled by L1 and L2 penalty terms. The parameter set with the best validation performance during the randomized search was selected as the city-specific hyperparameter configuration.

Model performance was evaluated using a five-fold random cross-validation strategy. For each city, valid hourly samples were randomly divided into five folds using a fixed random seed. In each iteration, four folds were used for training and the remaining fold was used for validation. The selected city-specific hyperparameters were kept fixed during the five-fold evaluation, and out-of-fold predictions were generated for all valid city-hour samples. This cross-validation strategy was used to evaluate the model's ability to reproduce hourly $PM_{2.5}$ variability within the study period, rather than to assess future-year forecasting skill.

The evaluation metrics included the correlation coefficient (R), coefficient of determination (R^2), root-mean-square error (RMSE), mean absolute error (MAE), and mean bias error (MBE). City-level metrics were calculated using the out-of-fold predictions for each city, and regional performance was evaluated by pooling all city-hour out-of-fold predictions across the 36 cities.

https://doi.org/10.5194/egusphere-2026-4127
Preprint. Discussion started: 31 August 2026

3.3 SHAP interpretation analysis

To interpret the LightGBM models and quantify the contribution of individual predictors, the Shapley Additive Explanations (SHAP) framework was applied. For each prediction, SHAP decomposes the model output into a baseline value and the additive contributions of all predictors:

$$f(x_i) = E[f(x)] + \sum_{j=1}^{m} \phi_{ij} \tag{6}$$

where $f(x_i)$ is the predicted $PM_{2.5}$ concentration for sample i, $E[f(x)]$ is the expected model output, m is the number of predictors, and ϕ_{ij} is the SHAP value of predictor j for sample i. A positive SHAP value indicates that the predictor increases the predicted $PM_{2.5}$ concentration relative to the expected output, whereas a negative value indicates a decreasing effect.

SHAP values were calculated for each city-specific LightGBM model in each cross-validation fold using TreeExplainer. For each fold, SHAP values were calculated on the validation subset. When the validation subset contained more than 3000 samples, 3000 samples were randomly selected to reduce computational cost. For each city-fold model, the SHAP-based importance of predictor (j) was calculated as the mean absolute SHAP value:

$$I_{jr} = \frac{1}{n_r} \sum_{i=1}^{n_r} \left| \phi_{ij}^{(r)} \right| \tag{7}$$

Where I_{jr} is the SHAP importance of predictor j in city-fold model r, n_r is the number of validation samples used for SHAP calculation in model r, and $\phi_{ij}^{(r)}$ is the SHAP value of predictor j for sample i in model r.

The overall regional SHAP importance was then obtained by averaging the city-fold SHAP importance values for each predictor:

$$I_j^{reg} = \frac{1}{R} \sum_{r=1}^{R} I_{jr} \tag{8}$$

where I_j^{reg} is the regional SHAP importance of predictor j, and R is the total number of valid city-fold models. Predictors were ranked according to I_j^{reg}, with larger values indicating stronger average contributions to $PM_{2.5}$ prediction. This SHAP-based ranking was used to identify the dominant temporal and meteorological drivers learned by the LightGBM models.

3.4 Meteorological normalization and $PM_{2.5}$ decomposition

https://doi.org/10.5194/egusphere-2026-4127
Preprint. Discussion started: 31 August 2026

After model evaluation, meteorological normalization was performed to estimate the $PM_{2.5}$ level expected under averaged meteorological conditions and to quantify the influence of actual meteorological variability. For each city, the optimal LightGBM hyperparameters identified in the Model training and cross-validation procedure subsection were used to retrain a final city-specific model using all valid hourly samples. Missing predictor values in the final modeling dataset were filled using the median values calculated from all valid samples of the corresponding city. The final model for city c is denoted as f_c^{final}

For a given city-hour sample i in city c, the final model was first applied to the observed meteorological feature vector and the temporal feature vector to obtain the $PM_{2.5}$ prediction under actual meteorological conditions:

$$\hat{PM}_{2.5,c,i}^{\mathrm{actual}} = f_c^{\mathrm{final}}\left(\mathrm{M}_{c,i}, \tau_{c,i}\right) \quad (9)$$

where $\mathrm{M}_{c,i}$ represents the meteorological feature vector, and $\tau_{c,i}$ represents the temporal feature vector, including the Unix timestamp, day of week, and month-cycle terms. The difference between observed $PM_{2.5}$ and the predicted $PM_{2.5}$ under actual meteorological conditions was retained as the model residual and was used only for diagnostic purposes.

To average out the influence of short term meteorological variability, the temporal features were kept unchanged, while the meteorological feature vector was replaced by randomly resampled meteorological vectors from the same city. For each city, B complete meteorological vectors were sampled with replacement from all valid hourly records, where B = 5000 in this study. Sensitivity tests with different resampling numbers showed that the weather-normalized $PM_{2.5}$ estimates became stable when B exceeded 3000, and B = 5000 was therefore used to ensure robust and reproducible estimates. Each resampled vector contained all meteorological variables from the same hour, rather than independently sampled values of individual variables. This strategy preserves the observed relationships among meteorological variables.

For each resampled meteorological scenario, the final model was used to predict $PM_{2.5}$ while retaining the original temporal feature vector:

$$\hat{PM}_{2.5,c,i}^{(b)} = f_c^{\mathrm{final}}\left(\mathrm{M}_{c,i}^{(b)}, \tau_{c,i}\right), \quad b = 1,2,\dots,B \quad (10)$$

where $\mathrm{M}_{c,i}^{(b)}$ is the b-th meteorological vector resampled from all valid hourly records of the same city, and $\tau_{c,i}$ is kept unchanged for the target city-hour sample.

The weather-normalized $PM_{2.5}$ component was calculated as the mean prediction over all resampled meteorological scenarios:

https://doi.org/10.5194/egusphere-2026-4127
Preprint. Discussion started: 31 August 2026

$$PM_{\mathrm{emi},c,i} = \frac{1}{B}\sum_{b=1}^{B} \hat{PM}_{2.5,c,i}^{(b)} \tag{11}$$

Here, $PM_{\mathrm{emi},c,i}$ represents the $PM_{2.5}$ level expected under averaged meteorological conditions for city c and hour i. It should not be interpreted as an emission inventory or direct emission amount. Instead, it is used as a weather-normalized, non-meteorological component that reflects emission-related and other slowly varying influences after short-term meteorological variability has been averaged out.

The meteorological modulation term was then calculated as:

$$PM_{\mathrm{met},c,i} = PM_{\mathrm{obs},c,i} - PM_{\mathrm{emi},c,i} \tag{12}$$

where $PM_{\mathrm{obs},c,i}$ denotes the observed $PM_{2.5}$ concentration. A positive $PM_{\mathrm{met},c,i}$ indicates that actual meteorological conditions increased $PM_{2.5}$ relative to the weather-normalized level, whereas a negative value indicates that meteorological conditions reduced $PM_{2.5}$. Monthly and annual values of PM_{obs}, PM_{emi}, PM_{met}, predicted $PM_{2.5}$ under actual meteorological conditions, and model residual were obtained by averaging the corresponding hourly values. Regional monthly and annual means were calculated by averaging all valid city-hour records within each period.

4. Annual trend and fire-activity comparison

4.1 Annual aggregation and trend analysis

Monthly and annual means of PM_{obs}, PM_{emi}, PM_{met}, $PM_{pred,actual}$, and model residual were calculated from the hourly city-level decomposition results. City-level monthly and annual values were obtained by averaging valid hourly values within each city and period, while regional means were calculated by averaging all valid city-hour records within the corresponding month or year. Annual linear trends of PM_{obs}, PM_{emi} and PM_{met}, were estimated from annual mean values using ordinary least-squares regression:

$$X_y = a + b \times y + \varepsilon_y \tag{13}$$

where $X_y$represents the annual mean value of PM_{obs}, PM_{emi} or PM_{met}, in year y, and b represents the annual trend slope.

4.2 External consistency analysis

To examine the relationship between weather-normalized $PM_{2.5}$ and biomass-burning activity, VIIRS active fire counts within 100 km of cities were compared with PM_{emi}at annual and monthly scales. At the annual scale, regional PM_{emi} and fire counts were converted to relative changes using 2015 as the baseline:

https://doi.org/10.5194/egusphere-2026-4127
Preprint. Discussion started: 31 August 2026

$$RC_y = \frac{X_y - X_{2015}}{X_{2015}} \times 100 \tag{14}$$

where RC_y represents the relative change (%) in year y, and X_y represents either annual PM_{emi} or annual fire counts.

At the monthly scale, the monthly fire count (F) was transformed as follows:

$$F_{\log} = \log(1 + F) \tag{15}$$

This logarithmic transformation was applied because fire counts are count-based and highly skewed, with many low-count months and a few high-count burning months. The addition of 1 allowed months with zero fire detections to be retained, while the transformation reduced the influence of extreme fire-count values. Same-month anomalies of $F_{\log}$ were then calculated by subtracting the long-term mean of the corresponding calendar month. PM_{emi} anomalies were calculated using the same approach. This anomaly-based comparison removes the regular seasonal cycle and focuses on whether months with higher-than-usual fire activity also correspond to higher-than-usual PM_{emi}. The monthly anomaly analysis was conducted for March, April, October, and November, which were identified as the major burning months. Linear regression and Pearson correlation were used to evaluate the relationship between PM_{emi} anomalies and fire-count anomalies during these months.

5. Results

5.1 Long-term improvement driven by anthropogenic emission reductions

Figure 1a shows the spatial distribution of long-term mean $PM_{2.5}$ concentrations across Northeast China during 2015–2025. The mean $PM_{2.5}$ concentration exhibited clear spatial heterogeneity, with higher values mainly found in central Liaoning, Harbin, and several industrial or densely populated cities, and lower values in northern Heilongjiang. The long-term city-level mean $PM_{2.5}$ concentration ranged from 17.705 μg m^{-3} in Daxinganling to 44.738 μg m^{-3} in Jinzhou, indicating substantial differences in the regional pollution baseline. Figure 1b presents the city-level trends in annual mean ground-level $PM_{2.5}$ concentrations from 2015 to 2025. A clear decreasing tendency was observed in most cities across Northeast China. Among the 36 cities, 34 exhibited negative trends, 30 of which were statistically significant ($p < 0.05$). The mean and median city-level trends were −1.742 and −1.860 μg m^{-3} yr^{-1}, respectively, with individual city trends ranging from −3.086 to 0.357 μg m^{-3} yr^{-1}. The strongest decreases were mainly found in Jilin and Liaoning provinces. Baishan showed the largest decline, with a trend of −3.086 μg m^{-3} yr^{-1}, followed by Shenyang (−2.969 μg m^{-3} yr^{-1}), Baicheng (−2.914 μg m^{-3} yr^{-1}), Anshan (−2.629 μg m^{-3} y^{r-1}), Siping (−2.555 μg m^{-3} yr^{-1}), and Tonghua (−2.543 μg m^{-3} yr^{-1}). At the provincial scale, the mean city-level $PM_{2.5}$ trend was −2.272 μg m^{-3} yr^{-1} in Jilin and −2.060 μg m^{-3} yr^{-1} in Liaoning, and all cities in these two provinces showed decreasing

https://doi.org/10.5194/egusphere-2026-4127
Preprint. Discussion started: 31 August 2026

$PM_{2.5}$ trends. In contrast, the decline was weaker in Heilongjiang, where the mean city-level trend was −1.033 μg m^{-3} yr^{-1}. YichunHLJ and Suihua were the only two cities with small positive trend estimates, but neither passed the $p < 0.05$ significance threshold. These two cities also showed different long-term $PM_{2.5}$ concentration levels, with a relatively low baseline in YichunHLJ and a higher baseline in Suihua. Therefore, the two non-significant positive estimates are not interpreted as a consistent increasing pattern. Rather, they indicate that $PM_{2.5}$ reductions were not evident in these two cities during the study period.

The regional annual statistics also presents the long-term improvement in $PM_{2.5}$ concentrations (Table S4). The regional annual mean $PM_{2.5}$ concentration decreased from 48.437 μg m^{-3} in 2015 to 29.201 μg m^{-3} in 2025, corresponding to a reduction of 39.713 %. The lowest annual mean $PM_{2.5}$ concentration occurred in 2022, with a value of 26.214 μg m^{-3}. The number of regional exceedance days declined from 52 d in 2015 to 12 d in 2025, and the cumulative city-level exceedance burden decreased from 2173 to 736 city-days. These findings indicate that the decrease in annual mean $PM_{2.5}$ was accompanied by a substantial reduction in both region-wide pollution episodes and cumulative city-level exceedance events. However, the decline was not strictly monotonic. Regional exceedance days increased to 40 d in 2017 and remained relatively high in 2019–2020, with 26 and 29 d, respectively, demonstrating that episodic pollution events still occurred despite the overall long-term improvement.

Prior to meteorological normalization, the LightGBM models were evaluated using out-of-fold predictions to verify that they could reproduce hourly $PM_{2.5}$ variability across Northeast China (Figure 2). Based on the full out-of-fold dataset, the overall R and R^2 between observed and predicted $PM_{2.5}$ were 0.902 and 0.803, respectively, with an RMSE of 17.220 μg m^{-3} and an MAE of 9.650 μg m^{-3}. R^2 values on city-level ranged from 0.648 to 0.838, and 35 of the 36 cities had R^2 values above 0.7. These results indicate that the model performance was sufficient for subsequent meteorological normalization and PM_{emi}–PM_{met} decomposition.

The meteorological-normalization results provide further insight into the drivers of the observed $PM_{2.5}$ decrease. As shown in Figure 3a, the PM_{emi} generally followed the long-term decline in observed $PM_{2.5}$. The linear trend of observed $PM_{2.5}$ was −1.734 μg m^{-3} yr^{-1}, close to the PM_{emi} trend of −1.656 μg m^{-3} yr^{-1}. This close agreement indicates that the long-term decline in observed $PM_{2.5}$ was largely retained in the weather-normalized component. In comparison, the PM_{met}, was much smaller in magnitude at the annual scale and primarily adjusted observed $PM_{2.5}$ around the PM_{emi} level (Figure 3b). PM_{met} was negative in most years, ranging from −5.345 μg m^{-3} in 2016 to −2.853 μg m^{-3} in 2015, indicating that annual meteorological conditions generally reduced $PM_{2.5}$ relative to PM_{emi}. The main exception was 2019, when PM_{met} became positive (1.239 μg m^{-3}) and coincided with an increase in observed $PM_{2.5}$ relative to adjacent years. These results suggest that, while meteorological variability interannual $PM_{2.5}$ fluctuations, the long-term decreasing trend was primarily driven by changes in $PM_{emi.}$

https://doi.org/10.5194/egusphere-2026-4127
Preprint. Discussion started: 31 August 2026

The spatial pattern of PM_{emi} trends further supports this interpretation (Figure 4a). Among the 36 cities, 34 showed negative PM_{emi} trends, of which 29 cities were statistically significant ($P<0.05$). The mean and median city-level PM_{emi} trends were −1.661 and −1.737 μg m^{-3} yr^{-1}, respectively, with values ranging from −2.965 to 0.610 μg m^{-3} yr^{-1}. The largest decreases were observed in Harbin (−2.965 μg m^{-3} yr^{-1}), Baicheng (−2.882 μg m^{-3} yr^{-1}), Baishan (−2.792 μg m^{-3} yr^{-1}), Shenyang (−2.698 μg m^{-3} yr^{-1}), Qitaihe (−2.694 μg m^{-3} yr^{-1}), and Tieling (−2.605 μg m^{-3} yr^{-1}). At the provincial scale, the mean PM_{emi} trend was stronger in Jilin (−2.009 μg m^{-3} yr^{-1}) and Liaoning (−1.963 μg m^{-3} yr^{-1}) than in Heilongjiang (−1.094 μg m^{-3} yr^{-1}). This spatial pattern was broadly consistent with that of observed $PM_{2.5}$ trends, indicating that cities with larger observed $PM_{2.5}$ reductions generally also experienced stronger decreases in the weather-normalized component. Therefore, the spatial heterogeneity of $PM_{2.5}$ improvement was closely associated with changes in PM_{emi} rather than with meteorological variability alone.

To further evaluate the emission-related interpretation of PM_{emi}, we compared PM_{emi} with independent CEDS $PM_{2.5}$ emission indices (Figure 4b, c). From 2015 to 2023, the normalized PM_{emi} values declined to 65.312. During the same period, the CEDS inventory values based on the summed emissions of BC, OC, SO_2, NO, and NH_3 decreased to 60.505, and the mean index of individually normalized species decreased to 64.355. PM_{emi} was strongly correlated with both CEDS indices, with R = 0.925 for the summed-species index and R = 0.882 for the mean-species index. The consistent decreases in PM_{emi} and independent anthropogenic emission indices indicate that the long-term improvement in $PM_{2.5}$ over Northeast China was closely linked to anthropogenic emission reductions, likely reflecting the effects of sustained air-pollution control policies, rather than being primarily driven by favorable meteorological conditions.

Nevertheless, the post-2022 period suggests that $PM_{2.5}$ reduction has entered a more challenging stage. The regional annual mean $PM_{2.5}$ reached its minimum of 26.214 μg m^{-3} in 2022, but remained nearly unchanged thereafter, at 29.200, 29.196, and 29.201 μg m^{-3} in 2023, 2024, and 2025, respectively. Meanwhile, PM_{emi} increased from 30.654 μg m^{-3} in 2022 to 34.088 μg m^{-3} in 2025. This indicates that the apparent stability of observed $PM_{2.5}$ after 2022 did not necessarily reflect a continued decline in the weather-normalized pollution baseline. Instead, fluctuations in PM_{emi} were partly offset by meteorological modulation in the observed $PM_{2.5}$ values. More importantly, the regional annual mean $PM_{2.5}$ after 2022 remained above the current annual standard of 25 μg m^{-3}, underscoring that Northeast China has entered a difficult stage of further $PM_{2.5}$ reduction. Therefore, although previous emission-control policies have substantially reduced $PM_{2.5}$ pollution in this region, additional anthropogenic emission reductions, especially from industrial, heating-related, and other combustion sources, are still needed to further lower the regional $PM_{2.5}$ baseline.

https://doi.org/10.5194/egusphere-2026-4127
Preprint. Discussion started: 31 August 2026

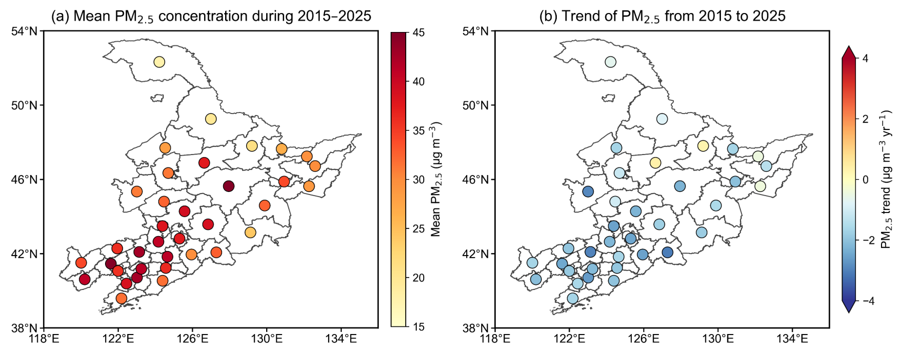

Figure 1. Spatial patterns of $PM_{2.5}$ concentrations and trends in Northeast China during 2015–2025. (a) City-level mean $PM_{2.5}$ concentrations averaged over 2015–2025. Circle colors indicate the long-term mean $PM_{2.5}$ concentration in each city. (b) City-level trends in annual mean $PM_{2.5}$ concentrations from 2015 to 2025. The trend for each city was estimated using linear regression of annual mean $PM_{2.5}$ concentration against year. Cooler colors indicate stronger decreasing trends, while warmer colors indicate weaker decreases or increasing tendencies. Units are μg m^{-3} for mean $PM_{2.5}$ concentrations and μg m^{-3} yr^{-1} for $PM_{2.5}$ trends.

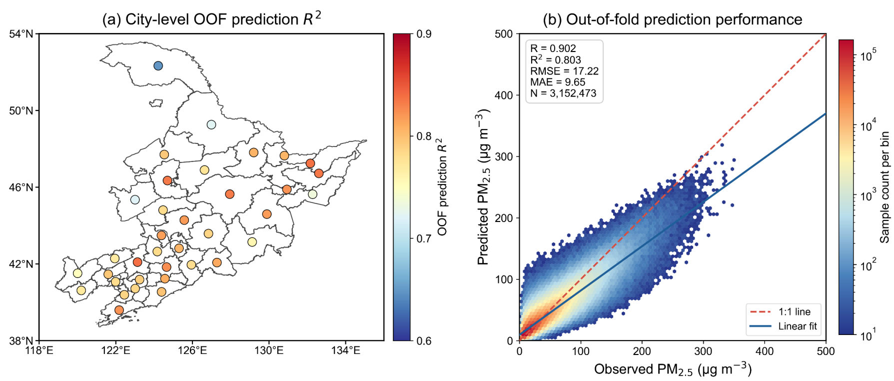

Figure 2. Performance of the LightGBM model for hourly $PM_{2.5}$ prediction. (a) Spatial distribution of city-level out-of-fold R^2 values across the 36 prefecture-level cities in Northeast China. Circle colors indicate city-level predictive performance. (b) Comparison between observed and out-of-fold predicted hourly $PM_{2.5}$ concentrations using the full out-of-fold dataset. Colors represent sample counts within two-dimensional bins on a logarithmic scale. The red dashed line denotes the 1:1 line, and the blue solid line denotes the linear regression fit. Inset statistics were calculated from the full out-of-fold dataset (N = 3,152,473).

https://doi.org/10.5194/egusphere-2026-4127
Preprint. Discussion started: 31 August 2026

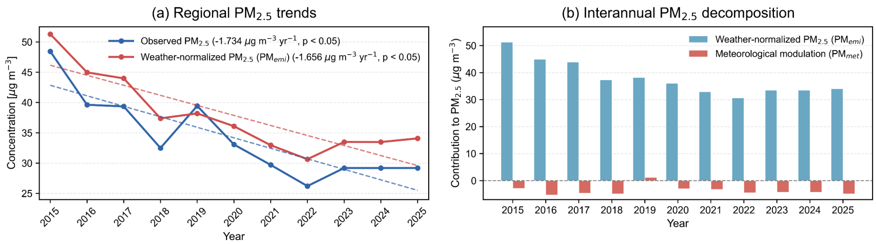

Figure 3. Interannual changes in observed $PM_{2.5}$, weather-normalized $PM_{2.5}$, and meteorological modulation in Northeast China during 2015–2025. (a) Regional annual mean observed $PM_{2.5}$ and weather-normalized $PM_{2.5}$ (PM_{emi}). Dashed lines indicate linear trends, with trend slopes and significance levels shown in the legend. (b) Interannual decomposition of regional $PM_{2.5}$ into the weather-normalized component PM_{emi} and the meteorological modulation term PM_{met}. Positive PM_{met} values indicate meteorological enhancement of $PM_{2.5}$ relative to the weather-normalized level, while negative values indicate meteorological reduction.

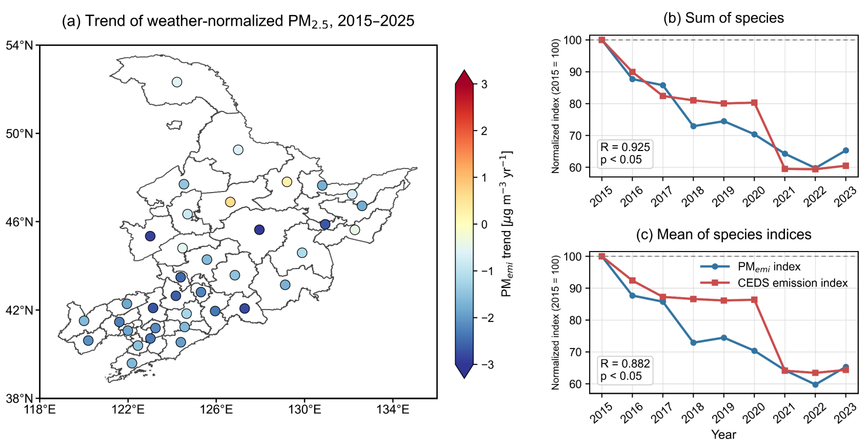

Figure 4. Spatial trends in weather-normalized $PM_{2.5}$ and comparison with CEDS emission indices. (a) City-level trends in weather-normalized PM2.5 (PM_{emi}) across Northeast China during 2015–2025. Circle colors indicate the linear trend slope of PMemi in each city. Negative values indicate decreases in PM_{emi}, while positive values indicate increases. (b) Comparison between the regional PM_{emi} index and the CEDS index based on the summed emissions of BC, OC, SO_2, NO, and NH_3 during 2015–2023. (c) Comparison between the regional PM_{emi} index and the mean CEDS index of individually normalized species. PM_{emi} and CEDS emissions were normalized to 2015. Correlation coefficients and significance levels are shown in panels (b)

https://doi.org/10.5194/egusphere-2026-4127
Preprint. Discussion started: 31 August 2026

and (c).

5.2 Meteorological amplification during regional $PM_{2.5}$ exceedance days

Although the preceding analysis demonstrates that meteorological modulation had a limited effect on the long-term declining trend of $PM_{2.5}$, its influence on short-term variability, especially during high-pollution episodes, was substantial. At the regional daily scale, PM_{met} was negative on 2935 of the 4011 days during 2015–2025, accounting for 73.174 % of all days. This indicates that, under most daily conditions, meteorology tended to reduce $PM_{2.5}$ relative to the weather-normalized level, likely through dilution, dispersion, or removal processes. However, this general pattern was reversed during regional high-pollution episodes.

Regional exceedance days were defined as days when the regional daily mean observed $PM_{2.5}$ exceeded 75 μg m^{-3}. The regional daily mean was calculated by averaging all valid hourly records across the 36 cities within each day. Based on this definition, 229 regional exceedance days were identified during 2015–2025. PM_{met} was positive on all 229 regional exceedance days, indicating that these exceedance events consistently occurred under meteorological conditions that enhanced $PM_{2.5}$ relative to the weather-normalized level. This contrast suggests that meteorology more often acted as a cleaner under normal conditions, but became an important amplification factor during regional $PM_{2.5}$ exceedance events.

For these exceedance days, daily PM_{obs}, PM_{emi}, and PM_{met} were calculated from the regional daily mean series and then summarized by year to examine the relative roles of the weather-normalized baseline and meteorological modulation during high-pollution episodes (Table S5 and Figure 5a). Averaged across all 229 regional exceedance days, with annual values weighted by the number of exceedance days in each year, the mean observed $PM_{2.5}$ concentration was 99.615 μg m^{-3}, with mean PM_{emi} and PM_{met} values of 58.019 and 41.596 μg m^{-3}, respectively. This indicates that exceedance episodes generally occurred under the combined influence of an elevated weather-normalized $PM_{2.5}$ baseline and unfavorable meteorological conditions. Because PM_{met} was positive on all regional exceedance days, the meteorological contribution should be interpreted as amplification conditional on exceedance events, rather than evidence that meteorology alone caused the exceedances.

The relative contributions of PM_{emi} and PM_{met} changed over time. In the early years, exceedance events were associated with a higher weather-normalized baseline. The mean PM_{emi} during exceedance days was 69.542 μg m^{-3} in 2015, 64.091 μg m^{-3} in 2016, and 61.536 μg m^{-3} in 2017. During 2015–2017, PM_{emi} alone exceeded 75 μg m^{-3} on 23 regional exceedance days, including 19 d in 2015, 1 d in 2016, and 3 d in 2017. After 2018, no exceedance day had PM_{emi} above 75 μg m^{-3}, indicating that the weather-normalized component alone was generally insufficient to exceed the daily standard in the later period.

https://doi.org/10.5194/egusphere-2026-4127
Preprint. Discussion started: 31 August 2026

In several later years, exceedance-day $PM_{2.5}$ was instead strongly amplified by meteorological modulation. For example, in 2019, the mean PM_{emi} during exceedance days was 48.574 μg m^{-3}, while PM_{met} reached 55.068 μg m^{-3}, resulting in a mean exceedance-day $PM_{2.5}$ concentration of 103.642 μg m^{-3}. A similar pattern occurred in 2024, when PM_{emi} was 47.069 μg m^{-3} and PM_{met} increased to 60.886 μg m^{-3}. The meteorological amplification fractions were 53.133 % in 2019 and 56.399 % in 2024. These results suggest that, after the decline in PM_{emi}, regional exceedance events were less often supported by the weather-normalized component alone and became more dependent on the superposition of unfavorable meteorological conditions.

SHAP analysis was further used to interpret the meteorological sensitivity learned by the LightGBM model. In the overall SHAP ranking, both meteorological and temporal predictors contributed to $PM_{2.5}$ predictions (Figure S2). Among the meteorological variables, T ranked first, followed by p_s, SSRD, T_d, wind components, RH, BLH, TP, and TCC. This indicates that the model captured the influence of multiple meteorological processes, including thermal conditions, synoptic-scale pressure variability, radiation, moisture, boundary-layer mixing, precipitation, and near-surface transport.

For regional exceedance-day samples, Figure 5b further shows the meteorological predictors that contributed positively to $PM_{2.5}$ during high-pollution episodes. The mean positive SHAP contributions were largest for T, followed by p_s and T_d, while wind components, RH, BLH, TP, TCC, and SSRD made smaller positive contributions. This exceedance-specific ranking suggests that thermal conditions, pressure-related synoptic variability, and atmospheric moisture were closely associated with $PM_{2.5}$ enhancement during regional exceedance events.

These SHAP results should be interpreted as model-based evidence of meteorological association rather than direct proof of a single physical mechanism. Nevertheless, the ranking is consistent with known conditions that favor $PM_{2.5}$ accumulation in Northeast China. Temperature is closely related to seasonal heating demand, near-surface stability, and secondary aerosol processes in this cold-region environment. Surface pressure can reflect synoptic patterns associated with weak ventilation and stagnant air, which limit horizontal dispersion. Dewpoint temperature is closely linked to atmospheric moisture, and its role is consistent with the effect of relative humidity on particle hygroscopic growth and secondary aerosol formation. Therefore, the exceedance-day SHAP results suggest that high $PM_{2.5}$ episodes tended to occur under a combination of meteorological conditions unfavorable for dispersion and favorable for particle accumulation, rather than being controlled by any single meteorological variable.

Overall, the exceedance-day results show that PM_{emi} and PM_{met} played different roles during regional $PM_{2.5}$ pollution episodes. PM_{emi} represented the weather-normalized baseline, whereas PM_{met} captured the additional meteorological modulation during exceedance days. Although meteorology reduced $PM_{2.5}$ relative to PM_{emi} on most regional days, all regional exceedance events occurred with positive PM_{met}. This contrast indicates that unfavorable meteorological

https://doi.org/10.5194/egusphere-2026-4127
Preprint. Discussion started: 31 August 2026

conditions were a key amplification factor during high-pollution episodes, especially after the decline in the weather-normalized $PM_{2.5}$ baseline.

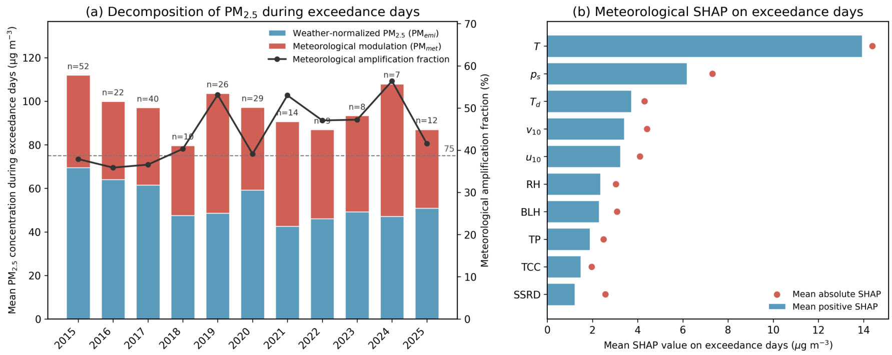

Figure 5. Meteorological amplification during regional $PM_{2.5}$ exceedance days in Northeast China. Regional exceedance days were defined as days when the regional daily mean observed $PM_{2.5}$ exceeded 75 μg m^{-3}, with regional daily means calculated by averaging all valid hourly records across the 36 cities. (a) Interannual decomposition of mean $PM_{2.5}$ concentrations during regional exceedance days into the weather-normalized component (PM_{emi}) and the meteorological modulation term (PM_{met}). Stacked bars show PM_{emi} and PM_{met}, and the black line denotes the meteorological amplification fraction, calculated as PM_{met} / $PM_{2.5}$ × 100 %. Numbers above the bars indicate the number of regional exceedance days in each year. The dashed horizontal line marks the daily $PM_{2.5}$ standard of 75 μg m^{-3}. (b) SHAP-based meteorological contributions during regional exceedance-day samples. Blue bars represent mean positive SHAP contributions, calculated as mean [max(SHAP_j, 0)], and red points represent mean absolute SHAP values. Only meteorological predictors were included in panel (b).

5.3 Episodic impacts of biomass burning in agricultural seasons

In addition to industrial and heating-related emissions, agricultural activities can also affect $PM_{2.5}$ variability in Northeast China. As one of the major grain-producing regions in China, Northeast China experiences intensive agricultural residue burning during specific periods before spring planting and after autumn harvest. Therefore, satellite-detected fire activity was further examined to evaluate the episodic influence of biomass burning on weather-normalized $PM_{2.5}$ variability.

The VIIRS active fire records showed a clear seasonal concentration of fire activity in Northeast China (Figure 6). March, April, October, and November together accounted for 69.4 % of the annual fire counts within 100 km of cities. April contributed the largest share (27.9 %), followed by March (15.7 %), November (13.4 %), and October (12.4 %). This seasonal pattern is consistent with the timing of agricultural residue burning before spring planting and after autumn harvest, suggesting that open biomass burning is an important episodic source of air-

https://doi.org/10.5194/egusphere-2026-4127
Preprint. Discussion started: 31 August 2026

pollution variability in Northeast China.

Using the annual relative change and burning month anomaly metrics described in the External consistency analysis subsection, PM_{emi} showed a positive association with satellite detected fire activity (Figure 7a). At the annual scale, the relative changes in PM_{emi} and fire counts were positively correlated ($R = 0.625$, $p < 0.05$). Both indicators generally declined after 2015, although their year-to-year correspondence was not uniform. This is expected because PM_{emi} represents the combined influence of multiple non-meteorological factors rather than biomass burning alone. Nevertheless, the positive correlation suggests that interannual changes in fire activity contributed to part of the weather-normalized $PM_{2.5}$ variability. The burning-month anomaly analysis provides a more focused comparison after removing the regular seasonal cycle (Figure 7b). For March, April, October, and November, PM_{emi} anomalies were positively correlated with log-transformed fire-count anomalies ($R = 0.658$, $p < 0.05$, $n = 44$). This result indicates that months with higher-than-usual fire activity tended to have higher-than-usual weather-normalized $PM_{2.5}$. Because PM_{emi} was derived after averaging out short-term meteorological variability, the positive anomaly relationship supports the contribution of biomass-burning activity to non-meteorological $PM_{2.5}$ variability during the main burning months.

The $PM_{2.5}$–CO relationship provides additional combustion-related evidence (Figure 7c,d). For all months from 2015 to 2025, regional monthly $PM_{2.5}$ and CO were strongly correlated ($R = 0.864$, $p < 0.05$, $n = 132$). A similarly strong relationship was found when only the main burning months were considered ($R = 0.796$, $p < 0.05$, $n = 44$). Since CO is produced by incomplete combustion, the consistent $PM_{2.5}$–CO relationship indicates that combustion-related sources were closely associated with $PM_{2.5}$ variability in Northeast China. During March, April, October, and November, this relationship is consistent with the influence of biomass burning, while CO may also reflect other combustion sources, such as residential fuel use, industrial combustion, and traffic emissions.

https://doi.org/10.5194/egusphere-2026-4127
Preprint. Discussion started: 31 August 2026

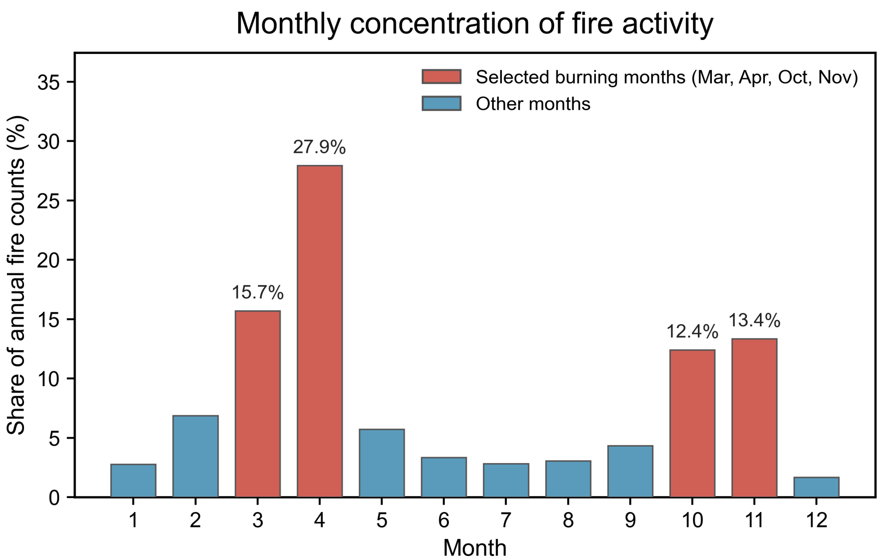

Figure 6. Monthly distribution of satellite-detected fire counts within 100 km of cities in Northeast China. Bars indicate the monthly share of annual fire counts. Orange bars denote the selected major burning months (March, April, October, and November), and grey-blue bars denote the remaining months.

https://doi.org/10.5194/egusphere-2026-4127
Preprint. Discussion started: 31 August 2026

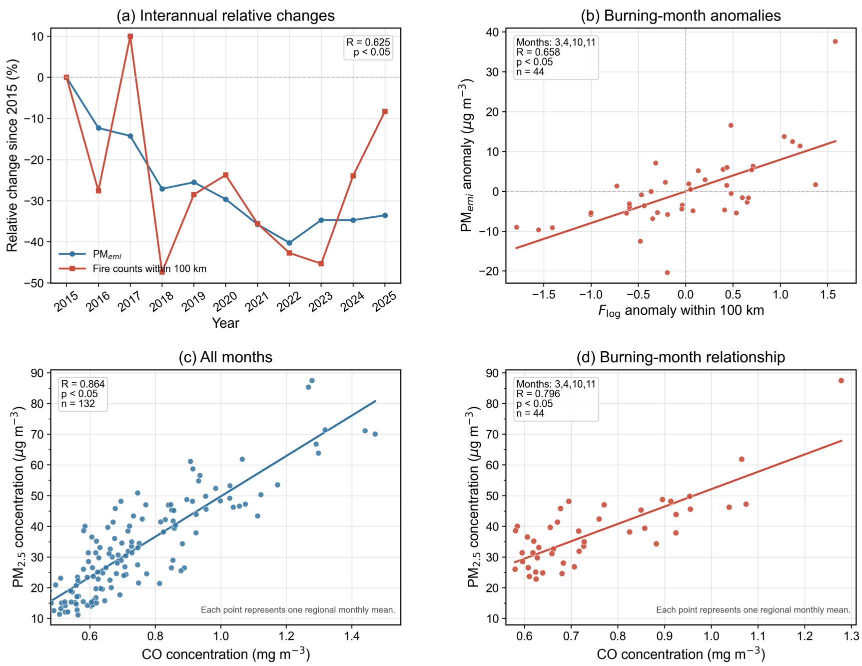

Figure 7. Associations between fire activity, CO, and $PM_{2.5}$ variability in Northeast China. (a) Interannual relative changes in weather-normalized $PM_{2.5}$ (PM_{emi}) and VIIRS fire counts within 100 km of cities, with both variables referenced to 2015. (b) Relationship between PM_{emi} anomalies and log transformed fire count anomalies during the main burning months, including March, April, October, and November. Monthly anomalies were calculated by removing the long term mean for the corresponding calendar month. (c) Relationship between regional monthly mean $PM_{2.5}$ and CO concentrations for all months from 2015 to 2025. (d) Relationship between regional monthly mean $PM_{2.5}$ and CO concentrations during the main burning months. Solid lines indicate linear regression fits. Correlation coefficients, significance levels, and sample sizes are shown in each panel.

6. Discussion

The results of this study show that $PM_{2.5}$ air quality in Northeast China improved substantially from 2015 to 2025. Both the observed $PM_{2.5}$ concentrations and the meteorologically normalized component PM_{emi} showed clear decreasing trends, and the PM_{emi} decrease was consistent with independent CEDS emission indices. These results suggest that the long term $PM_{2.5}$ reduction in Northeast China was closely related to anthropogenic emission reductions, reflecting the effectiveness of sustained policies for air pollution control. This finding is important for old industrial regions with a cold climate, where $PM_{2.5}$ pollution is strongly

https://doi.org/10.5194/egusphere-2026-4127
Preprint. Discussion started: 31 August 2026

influenced by industrial combustion, winter heating, and other fossil fuel sources.

The post 2022 period indicates that further $PM_{2.5}$ reduction has entered a more difficult stage. Although the regional annual mean $PM_{2.5}$ reached its lowest level in 2022, it remained nearly unchanged during 2023 to 2025 and was still above the annual standard of 25 μg m^{-3}. PM_{emi} also increased slightly after 2022, suggesting that the meteorologically normalized pollution baseline did not continue to decline. This does not mean that previous emission control policies were ineffective. Rather, it suggests that the marginal effect of existing measures may have weakened, and that the remaining $PM_{2.5}$ sources are more difficult to reduce. Future air quality management in Northeast China should therefore place more emphasis on persistent anthropogenic sources, including industrial emissions, winter heating, scattered fuel combustion, and other local combustion activities.

Meteorological conditions also need to be considered in future $PM_{2.5}$ management. This study found that PM_{met} was negative on most regional daily samples, indicating that meteorology often helped reduce $PM_{2.5}$ under normal conditions. PM_{met} was positive on all regional exceedance days, showing that unfavorable meteorological conditions consistently amplified $PM_{2.5}$ during pollution episodes. The SHAP results for exceedance days further suggest that thermal conditions, surface pressure, and moisture related variables were closely associated with $PM_{2.5}$ enhancement during these events. These findings indicate that emission control policies should be combined with meteorology based early warning and temporary control measures. During periods with stagnant conditions, weak dispersion, high humidity, or other unfavorable meteorological backgrounds, stricter short-term controls on industrial operations, heating emissions, traffic, and construction dust may help prevent regional exceedance events. This type of episode focused management will become increasingly important under stricter air quality standards.

Agricultural biomass burning remains another episodic source that requires control. VIIRS fire records showed two clear peaks in fire activity, one in March and April and the other in October and November, corresponding to the periods before spring planting and after autumn harvest. PM_{emi} was positively associated with fire activity during these burning seasons, and the relationship between $PM_{2.5}$ and CO further supported the influence of combustion related sources. The slight increase in PM_{emi} after 2022 also coincided with renewed fluctuations in fire activity, suggesting that agricultural burning may still contribute to short term $PM_{2.5}$ increases and variability in the weather-normalized $PM_{2.5}$ component. Therefore, controlling open biomass burning should remain an important component of regional $PM_{2.5}$ management. Strengthening straw collection and utilization, improving field burning supervision during key agricultural seasons, and combining satellite fire monitoring with local enforcement could help reduce short-term $PM_{2.5}$ increases and biomass-burning-related variability.

7. Conclusion

https://doi.org/10.5194/egusphere-2026-4127
Preprint. Discussion started: 31 August 2026

This study developed an explainable machine learning and weather normalization framework to investigate $PM_{2.5}$ variability across 36 prefecture-level cities in Northeast China from 2015 to 2025. Hourly $PM_{2.5}$ observations, ERA5 meteorological variables, LightGBM modeling, SHAP interpretation, and weather normalization were combined to separate observed $PM_{2.5}$ into a weather-normalized component (PM_{emi}) and a meteorological modulation term (PM_{met}). CEDS emission indices, VIIRS active fire detections, and CO observations were further used as independent indicators to evaluate the interpretation of PM_{emi}.

Three main findings emerged. First, regional annual mean $PM_{2.5}$ decreased from 48.437 μg m^{-3} in 2015 to 29.201 μg m^{-3} in 2025, corresponding to a reduction of 39.713%. Decreasing trends were observed in 34 of the 36 cities, and 30 were statistically significant. The regional PM_{emi} trend was −1.656 μg m^{-3} yr^{-1}, close to the observed $PM_{2.5}$ trend of −1.734 μg m^{-3} yr^{-1}, and PM_{emi} was strongly correlated with independent CEDS emission indices. However, both observed $PM_{2.5}$ and PM_{emi} showed limited further improvement after 2022, and the regional annual mean $PM_{2.5}$ remained above 25 μg m^{-3} during 2023–2025. Second, PM_{met} was negative on 73.174% of regional daily samples but positive on all 229 regional exceedance days. Across these exceedance days, mean observed $PM_{2.5}$, PM_{emi}, and PM_{met} were 99.615, 58.019, and 41.596 μg m^{-3}, respectively, indicating substantial meteorological amplification during pollution episodes. Third, 69.4% of annual VIIRS fire detections occurred in March, April, October, and November. The positive associations of PM_{emi} with fire activity, together with the relationship between $PM_{2.5}$ and CO, indicate that agricultural biomass burning and other combustion activities were closely linked to short-term $PM_{2.5}$ variability during the main burning seasons.

These results provide systematic evidence of the effectiveness of past air pollution controls in Northeast China, while also showing that further $PM_{2.5}$ improvement is increasingly constrained by persistent combustion emissions, agricultural biomass burning, and unfavorable meteorological conditions. Northeast China represents an important cold-climate region in which heavy industry, winter heating, and intensive agricultural activity coexist. Further air quality improvement will require continued reductions in industrial and heating emissions, stronger control of open biomass burning, and meteorology-informed management during pollution episodes. Future studies should integrate higher-resolution emission inventories, chemical transport modeling, and more source-specific chemical tracers to further distinguish the contributions of heating, industrial combustion, and agricultural burning and to evaluate the effectiveness of targeted control measures.

Data availability

The $PM_{2.5}$ and CO observations used in this study were obtained from the China National Environmental Monitoring Centre (https://www.cnemc.cn/). ERA5 meteorological reanalysis data are publicly available from the European Centre for Medium-Range Weather Forecasts (https://cds.climate.copernicus.eu). VIIRS active fire data are available from NASA FIRMS. CEDS emission data are publicly available from the Community Emissions Data System (https://www.pnnl.gov/projects/ceds).

Acknowledgements

This work is jointly supported by Excellent Young Scientists Fund of the National Natural Science Foundation of China (No.62322514), Anhui Science Fund for Distinguished Young Scholars (No.2308085J25), and National Key Research and Development Program of China (No.2023YFC3709502, No.2022YFC3700100).

Author contributions

H.Y and YW.S designed this study. ZF.P wrote the paper with help from H.Y and YW.S. ZF.P contributed to analysis of the data for this study. All co-authors commented on this study.

Competing interests

The contact author has declared that none of the authors has any competing interests.

References

WHO global air quality guidelines: particulate matter (PM2.5 and PM10), ozone, nitrogen dioxide, sulfur dioxide and carbon monoxide: https://www.who.int/publications/i/item/9789240034228, last access: 6 May 2025.

Bai, L., Li, C., Yu, C. W., and He, Z.: Air pollution and health risk assessment in Northeastern China: A case study of Jilin Province, Indoor Built Environ., 30, 1857–1874, https://doi.org/10.1177/1420326X20979274, 2021.

https://doi.org/10.5194/egusphere-2026-4127
Preprint. Discussion started: 31 August 2026

Chen, W., Zhang, S., Tong, Q., Zhang, X., Zhao, H., Ma, S., Xiu, A., and He, Y.: Regional Characteristics and Causes of Haze Events in Northeast China, Chin. Geogr. Sci., 28, 836–850, https://doi.org/10.1007/s11769-018-0965-3, 2018.

Grange, S. K., Carslaw, D. C., Lewis, A. C., Boleti, E., and Hueglin, C.: Random forest meteorological normalisation models for Swiss PM_{10} trend analysis, Atmospheric Chem. Phys., 18, 6223–6239, https://doi.org/10.5194/acp-18-6223-2018, 2018.

Hersbach, H., Bell, B., Berrisford, P., Hirahara, S., Horányi, A., Muñoz-Sabater, J., Nicolas, J., Peubey, C., Radu, R., Schepers, D., Simmons, A., Soci, C., Abdalla, S., Abellan, X., Balsamo, G., Bechtold, P., Biavati, G., Bidlot, J., Bonavita, M., De Chiara, G., Dahlgren, P., Dee, D., Diamantakis, M., Dragani, R., Flemming, J., Forbes, R., Fuentes, M., Geer, A., Haimberger, L., Healy, S., Hogan, R. J., Hólm, E., Janisková, M., Keeley, S., Laloyaux, P., Lopez, P., Lupu, C., Radnoti, G., de Rosnay, P., Rozum, I., Vamborg, F., Villaume, S., and Thépaut, J.-N.: The ERA5 global reanalysis, Q. J. R. Meteorol. Soc., 146, 1999–2049, https://doi.org/10.1002/qj.3803, 2020.

Hoesly, R. M., Smith, S. J., Feng, L., Klimont, Z., Janssens-Maenhout, G., Pitkanen, T., Seibert, J. J., Vu, L., Andres, R. J., Bolt, R. M., Bond, T. C., Dawidowski, L., Kholod, N., Kurokawa, J., Li, M., Liu, L., Lu, Z., Moura, M. C. P., O'Rourke, P. R., and Zhang, Q.: Historical (1750–2014) anthropogenic emissions of reactive gases and aerosols from the Community Emissions Data System (CEDS), Geosci. Model Dev., 11, 369–408, https://doi.org/10.5194/gmd-11-369-2018, 2018.

Hou, L., Dai, Q., Song, C., Liu, B., Guo, F., Dai, T., Li, L., Liu, B., Bi, X., Zhang, Y., and Feng, Y.: Revealing Drivers of Haze Pollution by Explainable Machine Learning, Environ. Sci. Technol. Lett., 9, 112–119, https://doi.org/10.1021/acs.estlett.1c00865, 2022.

Houdou, A., El Badisy, I., Khomsi, K., Abdala, S. A., Abdulla, F., Najmi, H., Obtel, M., Belyamani, L., Ibrahimi, A., and Khalis, M.: Interpretable Machine Learning Approaches for Forecasting and Predicting Air Pollution: A Systematic Review, Aerosol Air Qual. Res., 24, 230151, https://doi.org/10.4209/aaqr.230151, 2023.

Huang, H., Jin, Y., Sun, W., Gao, Y., Sun, P., and Ding, W.: Biomass Burning in Northeast China over Two Decades: Temporal Trends and Geographic Patterns, Remote Sens., 16, 1911, https://doi.org/10.3390/rs16111911, 2024.

Ke, G., Meng, Q., Finley, T., Wang, T., Chen, W., Ma, W., Ye, Q., and Liu, T.-Y.: LightGBM: A Highly Efficient Gradient Boosting Decision Tree, in: Advances in Neural Information Processing Systems, 2017.

Li, X., Ma, Y., Wang, Y., Liu, N., and Et., A.: Temporal and spatial analyses of particulate matter (PM 10 and PM 2.5) and its relationship with meteorological parameters over an urban city in northeast China, Atmospheric Res., https://doi.org/10.1016/j.atmosres.2017.08.023, 2017.

Liu, Y., Zhao, H., Ma, Y., Yang, H., Wang, Y., Wang, H., Zhang, Y., Zou, X., Wang, H., Wen,

https://doi.org/10.5194/egusphere-2026-4127
Preprint. Discussion started: 31 August 2026

R., Zhao, Z., and Quan, W.: Characteristics of particulate matter and meteorological conditions of a typical air-pollution episode in Shenyang, northeastern China, in winter 2017, Atmospheric Pollut. Res., 12, 316–327, https://doi.org/10.1016/j.apr.2020.09.007, 2021.

Lundberg, S. M. and Lee, S.-I.: A unified approach to interpreting model predictions, in: Proceedings of the 31st International Conference on Neural Information Processing Systems, 4768–4777, 2017.

Ma, J., Yu, Z., Qu, Y., Xu, J., and Cao, Y.: Application of the XGBoost Machine Learning Method in PM2.5 Prediction: A Case Study of Shanghai, Aerosol Air Qual. Res., 20, 128–138, https://doi.org/10.4209/aaqr.2019.08.0408, 2020.

Ma, Y., Zhao, H., Dong, Y., Che, H., Li, X., Hong, Y., Li, X., Yang, H., Liu, Y., Wang, Y., Liu, N., and Sun, C.: Comparison of Two Air Pollution Episodes over Northeast China in Winter 2016/17 Using Ground-Based Lidar, J. Meteorol. Res., 32, 313–323, https://doi.org/10.1007/s13351-018-7047-4, 2018.

Schroeder, W., Oliva, P., Giglio, L., and Csiszar, I. A.: The New VIIRS 375m active fire detection data product: Algorithm description and initial assessment, Remote Sens. Environ., 143, 85–96, https://doi.org/10.1016/j.rse.2013.12.008, 2014.

Sun, Y., Yin, H., Lu, X., Notholt, J., Palm, M., Liu, C., Tian, Y., and Zheng, B.: The drivers and health risks of unexpected surface ozone enhancements over the Sichuan Basin, China, in 2020, Atmospheric Chem. Phys., 21, 18589–18608, https://doi.org/10.5194/acp-21-18589-2021, 2021.

Vu, T. V., Shi, Z., Cheng, J., Zhang, Q., He, K., Wang, S., and Harrison, R. M.: Assessing the impact of clean air action on air quality trends in Beijing using a machine learning technique, Atmospheric Chem. Phys., 19, 11303–11314, https://doi.org/10.5194/acp-19-11303-2019, 2019.

Wang, Y., Ying, Q., Hu, J., and Zhang, H.: Spatial and temporal variations of six criteria air pollutants in 31 provincial capital cities in China during 2013–2014, Environ. Int., 73, 413–422, https://doi.org/10.1016/j.envint.2014.08.016, 2014.

Xiao, Q., Chang, H. H., Geng, G., and Liu, Y.: An Ensemble Machine-Learning Model To Predict Historical PM2.5 Concentrations in China from Satellite Data, Environ. Sci. Technol., 52, 13260–13269, https://doi.org/10.1021/acs.est.8b02917, 2018.

Xiao, Q., Zheng, Y., Geng, G., Chen, C., Huang, X., Che, H., Zhang, X., He, K., and Zhang, Q.: Separating emission and meteorological contributions to long-term $PM_{2.5}$ trends over eastern China during 2000–2018, Atmospheric Chem. Phys., 21, 9475–9496, https://doi.org/10.5194/acp-21-9475-2021, 2021.

Yang, G., Zhao, H., Tong, D. Q., Xiu, A., and Et., A.: Impacts of post-harvest open biomass burning and burning ban policy on severe haze in the Northeastern China, Sci. Total Environ., https://doi.org/10.1016/j.scitotenv.2020.136517, 2020.

https://doi.org/10.5194/egusphere-2026-4127
Preprint. Discussion started: 31 August 2026

Yin, H., Liu, C., Hu, Q., Liu, T., Wang, S., Gao, M., Xu, S., Zhang, C., and Su, W.: Opposite impact of emission reduction during the COVID-19 lockdown period on the surface concentrations of PM2.5 and O3 in Wuhan, China, Environ. Pollut., 289, 117899, https://doi.org/10.1016/j.envpol.2021.117899, 2021a.

Yin, H., Lu, X., Sun, Y., Li, K., Gao, M., Zheng, B., and Liu, C.: Unprecedented decline in summertime surface ozone over eastern China in 2020 comparably attributable to anthropogenic emission reductions and meteorology, Environ. Res. Lett., 16, 124069, https://doi.org/10.1088/1748-9326/ac3e22, 2021b.

Yin, H., Sun, Y., Notholt, J., Palm, M., and Liu, C.: Spaceborne tropospheric nitrogen dioxide (NO_2) observations from 2005–2020 over the Yangtze River Delta (YRD), China: variabilities, implications, and drivers, Atmospheric Chem. Phys., 22, 4167–4185, https://doi.org/10.5194/acp-22-4167-2022, 2022a.

Yin, H., Sun, Y., You, Y., Notholt, J., Palm, M., Wang, W., Shan, C., and Liu, C.: Using machine learning approach to reproduce the measured feature and understand the model-to-measurement discrepancy of atmospheric formaldehyde, Sci. Total Environ., 851, 158271, https://doi.org/10.1016/j.scitotenv.2022.158271, 2022b.

Yin, H., Meng, L., Richardson, A. D., Martin, M. V., Mao, J., Li, H., Gilligan, J. M., Bhattarai, H., and Tai, A. P. K.: Ozone mitigates extended growing season and enhanced vegetation greenness driven by environmental change, Nat. Commun., 17, 5445, https://doi.org/10.1038/s41467-026-71959-y, 2026.

Zhai, S., Jacob, D. J., Wang, X., Shen, L., Li, K., Zhang, Y., Gui, K., Zhao, T., and Liao, H.: Fine particulate matter ($PM_{2.5}$) trends in China, 2013–2018: separating contributions from anthropogenic emissions and meteorology, Atmospheric Chem. Phys., 19, 11031–11041, https://doi.org/10.5194/acp-19-11031-2019, 2019.

Zhang, J., Liu, L., Wang, Y., Ren, Y., Wang, X., Shi, Z., Zhang, D., Che, H., Zhao, H., Liu, Y., Niu, H., Chen, J., Zhang, X., Lingaswamy, A. P., Wang, Z., and Li, W.: Chemical composition, source, and process of urban aerosols during winter haze formation in Northeast China, Environ. Pollut., 231, 357–366, https://doi.org/10.1016/j.envpol.2017.07.102, 2017.

Zhang, Q., Meng, X., Shi, S., Kan, L., Chen, R., and Kan, H.: Overview of particulate air pollution and human health in China: Evidence, challenges, and opportunities, The Innovation, 3, 100312, https://doi.org/10.1016/j.xinn.2022.100312, 2022.

Zhang, R., Wang, G., Guo, S., Zamora, M. L., Ying, Q., Lin, Y., Wang, W., Hu, M., and Wang, Y.: Formation of urban fine particulate matter, Chem. Rev., 115, 3803–3855, https://doi.org/10.1021/acs.chemrev.5b00067, 2015.

Zhao, H., Che, H., Zhang, X., Ma, Y., Wang, Y., Wang, H., and Wang, Y.: Characteristics of visibility and particulate matter (PM) in an urban area of Northeast China, Atmospheric Pollut. Res., 4, 427–434, https://doi.org/10.5094/APR.2013.049, 2013.

https://doi.org/10.5194/egusphere-2026-4127
Preprint. Discussion started: 31 August 2026

Zhen, J., Guan, P., Yang, R., and Zhai, M.: Transport matrix of PM2.5 in Beijing-Tianjin-Hebei and Yangtze River Delta regions: Assessing the contributions from emission reduction and meteorological conditions, Atmos. Environ., 304, 119775, https://doi.org/10.1016/j.atmosenv.2023.119775, 2023.

Zheng, H., Kong, S., Zhai, S., Sun, X., Cheng, Y., Yao, L., Song, C., Zheng, Z., Shi, Z., and Harrison, R. M.: An intercomparison of weather normalization of PM2.5 concentration using traditional statistical methods, machine learning, and chemistry transport models, Npj Clim. Atmospheric Sci., 6, 214, https://doi.org/10.1038/s41612-023-00536-7, 2023.

Zhong, J., Zhang, X., Gui, K., Wang, Y., Che, H., Shen, X., Zhang, L., Zhang, Y., Sun, J., and Zhang, W.: Robust prediction of hourly PM2.5 from meteorological data using LightGBM, Natl. Sci. Rev., 8, nwaa307, https://doi.org/10.1093/nsr/nwaa307, 2021.